Journal of Engineering Research xxx (xxxx) xxx

Contents lists available at ScienceDirect

Journal of Engineering Research

journal homepage: www.journals.elsevier.com/journal-of-engineering-research

Deep learning-based image segmentation for highwall stability monitoring in open pit mines

Tebogo M. Letshwiti, Mahdi Shahsavar, Amin Moniri-Morad, Javad Sattarvand *

Department of Mining and Metallurgical Engineering, University of Nevada, Reno, USA

ARTICLE INFO

Keywords:
Highwall crack monitoring
Deep learning
High-resolution imagery
U-Net

ABSTRACT

Current highwall monitoring methods are effective in tracking mass slope movements but often fail to adequately assess the dynamic impact of mining operations on highwall stability, particularly concerning the impact of rock fragmentation techniques, which can lead to structural instability and hazardous rockfall events. This study proposes a novel approach that leverages high-resolution imagery and deep learning-based U-Net segmentation model for automatic detection of cracks and fractures on highwalls in open pit mines. The developed methodology involves five key phases: obtaining high-quality imagery, pre-processing the acquired data, utilizing the U-Net image segmentation model, generating segmentation masks, and identifying cracks and fractures. Robustness testing was then conducted, comparing three U-Net model training configurations and the canny edge detector for crack segmentation. The results revealed that the model trained on a combination of original and augmented images achieved superior performance, boasting a 97 % accuracy, an intersection over union (IoU) of 0.77, and identifying cracks and fractures closely resembling the ground truth. This innovative approach not only enhances the efficiency of highwall monitoring but also minimizes the risk of hazardous incidents, thereby significantly improving safety standards and the overall impact on operational effectiveness in open-pit mining operations.

Introduction

Efficient highwall monitoring is crucial for ensuring the safety and stability of the surrounding environment in open pit mining operations, particularly considering the dynamic impact of mining activities. Existing techniques for monitoring slope movements have demonstrated their efficacy by offering uninterrupted observation to identify possible dangers. Nevertheless, these techniques have constraints when it comes to evaluating the extent of harm resulting from mining operations, such as the existing features of the ground, including faults and joints. These deficiencies heighten the likelihood of highwall damage and rockfall incidents, endangering both individuals and operations.

Although the implementation of drilling and blasting in the mining industry has greatly enhanced rock fragmentation, the dynamic impact of explosives for rock breakage poses drawbacks that the mining sector aims to address. Rock conditions, including geologic structure, rock alterations, and groundwater content, along with drill and blasting practices, can result in unfavorable ground conditions in mining highwalls. Due to the potential consequences of drilling and blasting, it is crucial to consistently monitor the highwall to ensure safety for future operations.

The mining process is divided into 4-unit operations [1], with drilling and blasting as two of them. Understanding the influence of these unit operations on highwall conditions requires a thorough understanding of the in-situ rock conditions. Data collection during prospecting and exploration will provide valuable insights into the ground conditions, thereby enhancing understanding of how activities such as drilling and blasting influence rock fragmentation. If the drilling and blasting practices are not well aligned with the ground conditions, certain outcomes can be expected that are undesirable and can have a detrimental effect on highwall structural integrity. Backbreak is one of these outcomes, it is the excessive breakage of rock due to blasting beyond a predetermined threshold, usually, the final row of drillholes [2]. Backbreak in highwall sections can lead to weakened areas, resulting in over-mining by shovels or material loss, ultimately causing rockfall events. Backbreak may occur due to poor blast planning or the existence of excessive geologic structures such as faults, joints, and shear zones. Table 1 gives the potential levels of damage to an open pit highwall caused by blasting. It is clear from the table that different damage levels appear differently on the pit highwalls and through visual inspection, we can determine how badly the highwall is damaged.

* Correspondence to: 1664 N. Virginia St., Reno, NV 89557, USA.
E-mail address: jsattarvand@unr.edu (J. Sattarvand).

https://doi.org/10.1016/j.jer.2025.04.002
Received 23 April 2024; Received in revised form 27 March 2025; Accepted 9 April 2025
Available online 9 April 2025

Please cite this article as: Tebogo M. Letshwiti et al., *Journal of Engineering Research,* https://doi.org/10.1016/j.jer.2025.04.002

Table 1
Levels of damage to pit walls produced by blasting [3].

Arbitrary damage level	Observed conditions of the wall		
	Joints & blocks	Dip angle appearance and conditions of face	Digging condition at face
1. Slight	Joints closed, infilling still welded	> 75° If used, semi-circular sections of wall control holes seen	Scars of shovel teeth seem in softer formation, further digging not practical
2. Moderate	Weak joint infilling is broken, occasional blocks and joints slightly displaced	> 65° Face is smooth, some hole sections seen. Mine cracks	Some free digging possible, but teeth 'chatter'
3. Heavy	Some joints dislocated and displaced	> 65° Minor spalls from face. Radial cracking seen	free digging possible > 5 ft with some effort
4. Severe	Face shattered, joints dislocated. Some blocks disoriented	> 55° Face irregular, some spalls, some backbreak cracks	free digging possible < 10 ft
5. Extreme	Blocks dislocated and disoriented, blast-induced fines observed	55° > 37° Face highly irregular, heavy spalling from face, large backbreak cracks	Extensive free digging possible > 10 ft

Related work

This study organizes the literature review into three categories: an overview of highwall monitoring methods, an in-depth exploration of the visual inspection method as the most effective approach, and an examination of the edge detection process in highwall monitoring. Subsequently, each of these three components is detailed in the following sub-sections.

Highwall monitoring methods

For highwall monitoring, an effective monitoring system should prioritize safe operational practices, early detection of instabilities, and enhanced geotechnical information on slope behavior in open pit mining. A recent study [4] suggests that monitoring techniques can be categorized into three groups: visual inspections, surface measurement and subsurface measurement.

Surface measurements employ techniques and equipment positioned on the earth's surface, such as highwalls, benches, or haul roads. These measure the geometry of rock slopes and detect any unnoticed rock movements. Survey Networks, tension crack mapping, surface wire extensometers, and equipment like total stations, prisms, radar, laser scanners, terrestrial lidar, and wireline extensometers are some of the methods in this area [4,5]. A survey network consists of strategically positioned target prisms on pit highwalls in areas prone to instabilities, along with non-moving control points for survey stations [6]. The system measures angles and distances between survey stations and target prisms to track the movement of slopes or highwalls and sends out warnings when necessary. Tension cracks form at the top of slopes or highwalls, indicating that the stress there exceeds the rock's strength. Crack width and direction must be monitored and measured to assess crack propagation and determine the unstable area [4,6]. Wire extensometers are devices that measure rock deformation or displacement under different loads or conditions [7]. Examples of other emerging technologies being used for surface measurements include radar monitoring devices used for slope stability assessment such as Slope Stability Radar (SSR), and terrestrial laser scanning. These technologies enable continuous scanning and comparison of high-resolution measurements of slope faces for any movement, regardless of magnitude [5,8].

Sub-surface measurements are typically collected using equipment placed below the ground such as in boreholes, to assess subsurface rock movement. The equipment used includes inclinometers, and borehole extensometers. Inclinometers measure subterranean rock displacement by placing a casing into the ground where movements are expected, and a displacement profile is derived from sensor data [6]. A borehole extensometer uses tensioned rods anchored at various points in the borehole. The displacement of the rock mass is measured by observing changes in the distance between the anchor and the rod head.

Finally, for the visual inspection method, the geotechnical engineer must regularly inspect the pit, accessways, highwalls, and crests near working areas to ensure safety for people, equipment, and mine operations [4]. During inspections, it is important to compare the current inspection with the previous one and document any changes that could negatively impact highwall stability. The utilization of emerging technologies such as survey drones, computed tomography (CT) scanning, photogrammetry, virtual reality, and teleoperation can greatly enhance safety and monitoring efficiency in mines [9–11].

Among the three monitoring methods mentioned above, the visual inspection method, when augmented with survey drones, enables a swift and immediate assessment of highwall fractures and cracks immediately following the blasting.

Visual inspection method

Limited research work has been done in the area of improving the visual inspection method of highwall monitoring. Most of the work done in this area either focuses on predicting how the mining operations affect the ground around it or using drill core data and images to identify faults, and discontinuities, and further characterize the rock mass. Bamford et al. [12] in their study introduce UAV systems for efficient, continuous monitoring of the blasting process in open pit mines, overcoming the limitations of traditional manual and intermittent methods. Their field experiments across various mines assessed aspects such as blast dynamics using a UAV-based approach in three stages: pre-blasting, during blasting, and post-blasting. The UAVs mapped pit walls for structural data and monitored blasthole patterns, while a high-speed camera on the UAV captured blast initiation and sequencing. The research underscores the potential of UAVs to enhance the quality of the blasting process, providing comprehensive insights for operational improvements, and includes recommendations for maximizing the value of UAV applications in blasting process monitoring. Gomez et al. [13] looked at using drones to enhance the visual inspection of tailings facilities by identifying the erosion areas of tailings dams. In [14], the researchers developed a flight planning application that relied on battery consumption data of UAVs to determine the optimal flight path for obtaining high resolution images of open pit highwalls. One researcher explored the utilization of drill core images for assessing the Rock Quality Designation (RQD) of rock formations [15]. The researchers employed a standard Convolutional Neural Network (CNN) with four convolutional layers. They utilized hyperparameter optimization to determine optimal user-selected parameters for configuring the CNN model. Xu et al. [16] propose a task-aware meta-learning (TSAML) paradigm for multi-type structural damage segmentation using limited images. Their method enhances task generation with feature density clustering, improves generalization by utilizing a dual-stage optimization process, and outperforms conventional U-Net and MAML (Model-Agnostic Meta-Learning)-based approaches. The study demonstrates robust segmentation accuracy across various damage types but notes some limitations in handling rare damage categories due to limited training samples. Also, because of the wide range of damage categories the study attempts to cover, the crack images used have little variability in terms of roughness and noise. In another study, Xu et al. [17] present a DeepLabv3 + -based model with MobileNetV2 as a lightweight backbone, for structural damage segmentation in bridges, reducing

parameters by 91.5 % and recognition time by 38.9 % while achieving 0.776 (mean Intersection over Union) mIoU. Their approach improves sensitivity to tiny cracks and robustness to complex backgrounds using depth wise separable convolutions, a refined ASPP module, and a piecewise loss function. However, limitations include reduced accuracy in highly complex backgrounds and the need for fine-tuning on new damage types. Future work aims to develop generalized models with fewer labeled images. Xu et al. [18] proposed a modified U-Net for detecting tiny cracks in high-resolution bridge images using a Self-Attention-Self-Adaption (SASA) neuron and a crack-specific data augmentation method (CRED). Their enhancements improved IoU by 29.8 % over standard U-Net, highlighting the value of architectural and augmentation strategies for fine-scale crack segmentation.

Valencia et al. [19] explored the application of support vector machines (SVM) and CNNs for precise drillhole detection in images and evaluated the agreement between the detected locations and the intended designs. This aids engineers in assessing the alignment between drilled drillholes and the design parameters. It enables them to make necessary adjustments to other parameters, such as the amount of explosive used, to maintain the desired outcome, despite any drilling errors. Peik et al. [20] used images to create high-definition 3D mesh objects to feed into a three-dimensional analytical program to simulate the trajectory of rocks down open pit highwalls during rockfall events. The studies described above have some limitations, the CNN model produces decent results when working with grid-like data such as images in image recognition and classification scenarios, but CNN models in most studies lacks the granularity needed to identify and quantify cracks effectively. Other deep learning methods including U-Net [21,22], Deep U-Net, Res U-Net, and Dense Net [23] perform semantic segmentation which is more proficient at identifying objects in images compared to image classification and recognition.

Semantic segmentation is a computer vision method used for image processing. It performs pixel-level labeling of images using object labels to identify objects in the image [24]. Image segmentation has seen limited use in the mining sector. A researcher utilized the Region-based Convolutional Neural Network (R-CNN) model to segment fractures in drill cores, potentially indicating actual geologic structures. R-CNN is an instance segmentation model that performs object detection, classification, and segmentation by integrating object detection and semantic segmentation [25]. Tension cracks, discussed before, are a significant focus of slope monitoring. Winkelmaier et al. [26] employed aerial imaging and U-Net and E-Net machine learning models to detect these cracks occurring on mine bench crests. The models excelled in localizing mine benches but faced challenges in identifying tension cracks. This limitation is significant for this study because proper monitoring of tension cracks requires accurate localization and observation of their growth over time.

Blasting efficacy is assessed on the following outcomes: rock fragmentation, backbreak, flyrock, and ground vibrations. Many researchers have explored these outcomes and attempted to link them to input parameters using machine learning and mathematical optimization techniques. The typical workflow in these research areas involves using drill and blasting parameters as inputs for a machine learning model, often a variation of neural networks. Optimization methods like genetic algorithm (GA) [27,28], ant colony optimization (ACO) [29], bee colony optimization (BCO) [30], ANN [31,32], particle swarm optimization (PSO) [33], and hybrid methods [34–37] are then used to optimize the selection of hyperparameters for the best results from the ML model. These studies focus on the selected parameters during the blasting operation and do not include visual analysis of the blasting outputs to address their alignment with the numerical values.

When examining the use of novel approaches such as locating cracks and fractures on highwall images using deep learning methods, it is crucial to compare with older methods of segmenting different regions in an image to identify objects, edge detection was selected as one of the measures of comparison for this study. Edge detection is a fundamental technique in computer vision. It aids in various visual tasks such as image recognition, segmentation, face recognition, medical tracking, and more [38]. Edge detection in computer vision involves capturing properties like discontinuities in the photometric, geometric, and physical characteristics of objects in images [39]. A 2-D filter convolves the input image, detecting significant pixel value changes while ignoring uniform regions [39]. Various edge detection methods have been developed, including Sobel, Prewitt, and Canny edge detectors, which have demonstrated advantages in different applications [40]. The Canny edge detector applies a Gaussian filter to reduce noise and then calculates the gradient magnitude and direction. If the magnitude of the gradient of a pixel is greater than the magnitudes of its two neighboring pixels in the direction of the gradient, classify the pixel as an edge. Otherwise, classify the pixel as the background [41].

For edge detection methods to be effective, they must be coupled with other image preprocessing techniques. Image enhancement, followed by binarization or histogram equalization can be an effective combination of preprocessing methodology. Image enhancement improves image quality for better downstream processing [42]. The available techniques in this area can be classified into spatial domain and frequency domain methods. Spatial domain techniques operate at the pixel level of the image, while frequency domain methods are applied on the Fourier transform of the image. Various studies [39–41] and practical solutions for edge detection primarily utilize spatial domain methods due to their interpretability, simplicity, and low complexity [42]. To binarize an image, a threshold value is required, pixels with values above the threshold are set to a maximum value, while those below the threshold are set to zero. Eq. 1 defines *dst* as the destination image, *src* as the source image, *thresh* as the threshold value, and *maxVal* as the value for setting pixels above the threshold [43].

$$dst(x, \quad y) = \begin{cases} \max Val \ if \ src(x, \quad y) & > thresh \\ 0 otherwise \end{cases} \tag{1}$$

After completing the mentioned preprocessing steps, edge detection can be conducted, which will segment off the cracks and fractures with strong edges that the edge detection process can identify.

Scope and objectives

The literature review highlighted the effectiveness of existing monitoring techniques, such as visual inspections, surface measurement, and subsurface measurement, in identifying potential dangers associated with slope movements. However, these methods face limitations when assessing the dynamic impact of mining operations on the highwall and the resulting cracks and fractures induced by mining operations, particularly in the presence of ground features like faults and joints. These limitations increase the risk of highwall damage and rockfall incidents, posing threats to both personnel and mining operations. Recognizing the shortcomings of current monitoring systems, a more sophisticated strategy is imperative to accurately assess the impact of mining operations and mitigate associated risks on highwalls. In response to these challenges, this study proposes an innovative technique that integrates one of the newly emerged technologies in mining, UAVs, with one of the advanced deep learning image processing algorithms, the U-Net image segmentation model, to advance highwall monitoring capabilities and dynamically analyze the impact of mining operations on highwall integrity. The contributions of this study are outlined as follows:

– Developing an automated system for detecting the impact of rock fragmentation techniques on cracks to proactively enhance safety measures, mitigating potential catastrophic incidents for both personnel and mining operations.

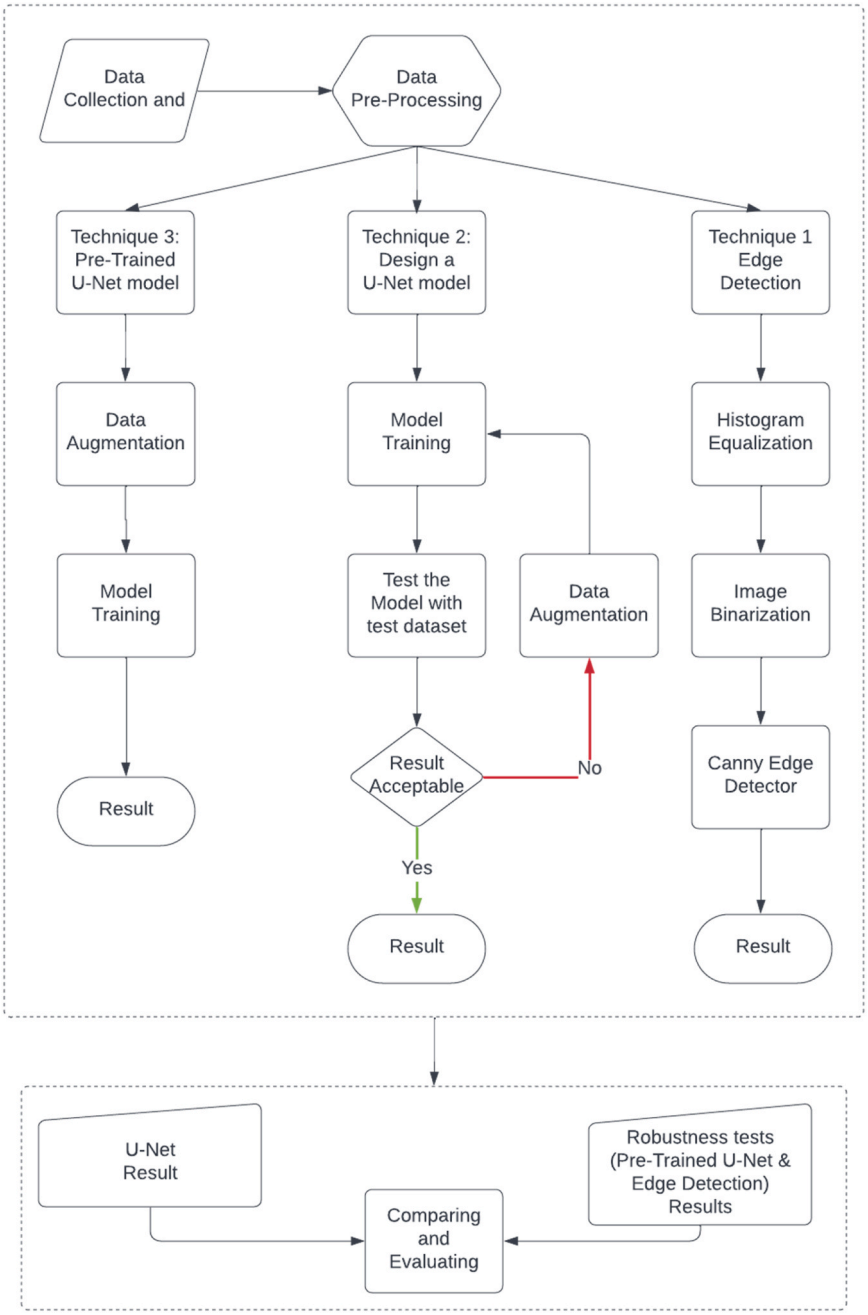

Fig. 1. Outline of the proposed methodology for this study.

- Unlike conventional methods that rely on labor-intensive processes and only monitor select highwalls, the proposed approach offers real-time analysis of the entire mine's highwalls.
- Demonstrating the capability of the proposed novel deep learning techniques in enhancing the safety of mine operations, achieving high test and validation accuracy.
- Utilizing the proposed methodology for highwall stability assessments and reinforcement decisions enables more precise decision-making, enhancing safety measures and reducing costs by avoiding unnecessary reinforcement efforts.

Materials and methods

This section revolves around the research approach for this study. Fig. 1 depicts the proposed approach for locating and segmenting cracks and fractures in images collected from mines' highwalls. As shown in Fig. 1, the first step involves data collection process. This step includes the selection of data collection locations, UAVs, and necessary software for aerial photogrammetry. Next is the data pre-processing step that prepares the image data for processing through the U-Net segmentation model and the edge detection process. The edge detection process is employed to demonstrate the efficiency of novel deep learning models in comparison with traditional visual inspection and image processing methods. Edge detection methods locate the presence of cracks or fractures by identifying significant changes in image pixel values. This process requires some image enhancement techniques to get the best edge detection results. We initially trained our U-Net model using the original dataset, but the results were unsatisfactory. Therefore, we applied image augmentation to enhance our data and conducted a second training session. Additionally, we explored a third approach using a pre-trained U-Net model designed for a similar problem. The outcomes of these three training strategies will be assessed using standard

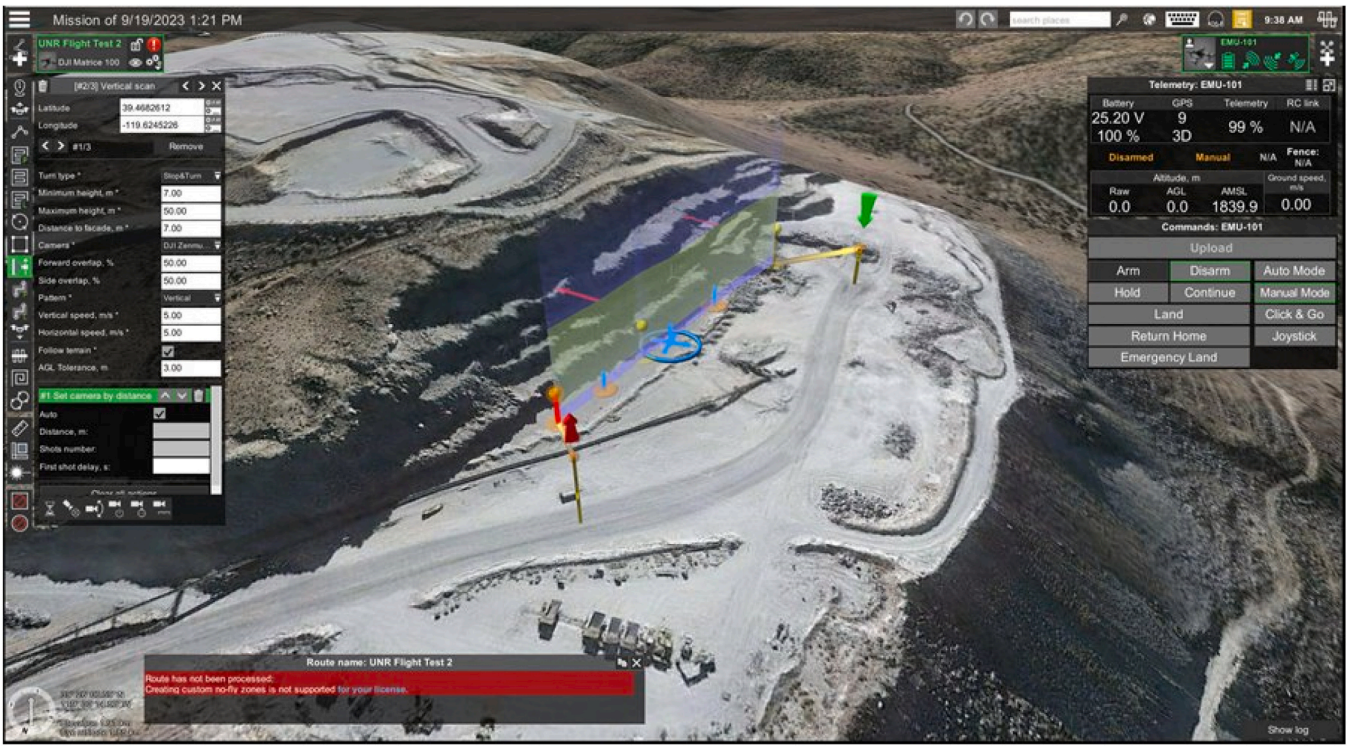

Fig. 2. A schematic view of the analyzed area.

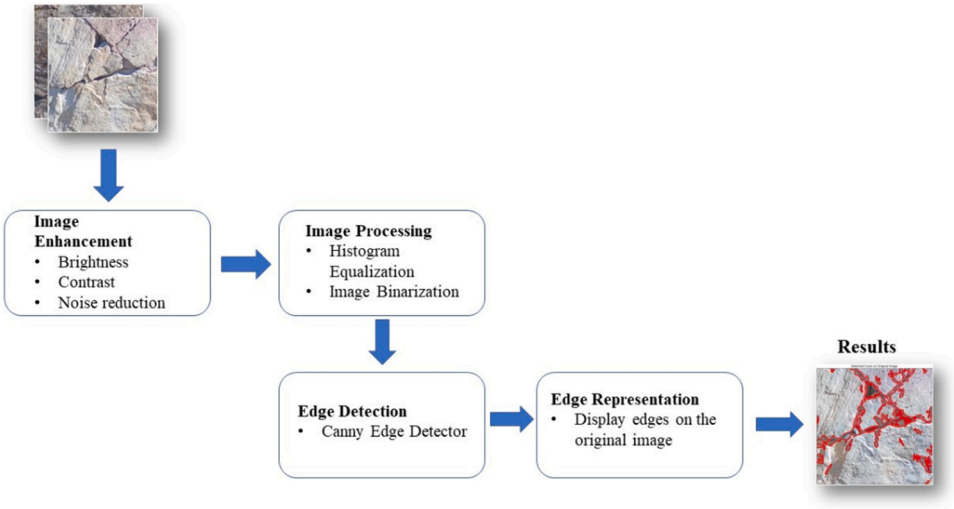

Fig. 3. Edge detection process.

evaluation metrics: precision, recall, F1 score, and Intersection over Union (IoU).

Data collection

Data was gathered at an aggregate quarry situated in Nevada, USA. The process was done using UAVs. For this study, three drones were selected: Phantom 4, Mavic Pro, and Matrice 100. The choice was made based on the drones' availability and the objective of examining if images captured by different cameras and drones would provide different outcomes during the segmentation phase. In recent years, drones provide faster, more efficient, and safer means for collecting data, the authors decided to use it for this study. Conducting aerial surveys of highwalls with drones can be difficult because of the restricted camera angles and flight paths that make it impossible to maintain a 90° angle with vertical features for surveys in the vertical plane.

The application employed in this study incorporates a distinctive vertical inspection tool that differs from the conventional practices in the mining industry. With the utilization of this tool, it is effortless to build a flight trajectory that encompasses the whole vertical surface of the highwall. This allows for the acquisition of high-resolution images at a 90° angle with the highwall, guaranteeing precise capture of the majority of the high wall's characteristics. Fig. 2 depicts a schematic view of the area where the drones flew to capture images.

Data pre-processing

Data pre-processing is a laborious but crucial component of this

investigation, ensuring the deep learning systems are trained efficiently. It involves confirming the availability of adequate training data and validating that this data meets the input criteria, including dimensions, image resolution, and data format. The first step was examining the gathered images to verify the presence of cracks or fractures, which is the focus of this study. Subsequently, we validated the dimensions of the images to be used as input for a U-Net semantic segmentation model. Deep learning neural networks can handle a variety of image sizes, including those ranging from 128 × 128 pixels to 256 × 256 pixels, and even images with larger sizes. Different drones used during data collecting resulted in the acquisition of various image sizes. Image cropping will be done to achieve the desired image dimensions of 640 x 640 pixels without compromising the quality of the images. Algorithm 1 below outlines the process followed to achieve this image cropping, while preserving the image quality. Once the images have been cropped, they undergo image annotation.

Algorithm 1. Image Cropping of Large Images

1. Input

- Image dataset $I = \{I_1, I_2, ..., I_n\}$, where each I_i is an input image.
- crop size $B \times B$ (default: 640 × 640).
- Output directory for storing image tiles.

2. Output

- Cropped image dataset $I' = \{T_1, T_2, ..., T_m\}$, where each T_j is a cropped image.

3. Procedure

1. Initialize directories:
   - Set input directory for images and output directory for cropped images.
2. Iterate through each image I_i in the dataset:
   - Load the image and extract its dimensions (height H, width W).
   - Determine the number of cropped images:
     - Compute number images across the vertical: $V = \lfloor H / B \rfloor$
     - Compute number of images across horizontal: $H = \lfloor W / B \rfloor$
   - Crop the image by iterating over non-overlapping $B \times B$ blocks:
     - Extract sub-image crop T_j from (row, col) → (row + B, col + B).
     - If T_j exceeds image boundaries, adjust dimensions accordingly.
   - Store each cropped image:
     - Assign unique filenames to T_j.
     - Save T_j to the output directory.
3. Repeat until all images are cropped.
4. End Algorithm

Preprocessing also included augmentation and normalization. Image augmentation is a technique used to create additional data samples by applying transformations to existing images. These transformations include random cropping, rotation, image mixing, brightness adjustment, noise injection, and flipping. However, not all augmentation methods are universally effective for training in all scenarios. In this study, random cropping, random rotation, and brightness adjustment were employed. Image cropping has two main functions: maintaining image resolution while achieving the desired image size and augmenting the dataset by increasing its size.

To effectively train an image segmentation model such as the U-Net, two essential components are needed: the input images and the ground truth masks. A ground truth mask is a visual representation that assigns labels or classes to each individual pixel in an input image. These masks provide the correct output for the network to learn from during the training process. They provide a comprehensive and precise understanding of the objects or regions present in the scene at a pixel level. Image annotation is the process of constructing a segmentation mask, which involves labeling or marking certain regions or pixels inside an image to identify their semantic category or class. The masks are usually binary, and in this study, we used binary masks as well. Pixels associated with cracks or fractures will be assigned a label of one, while the background and any unrelated items will be assigned a label of zero.

Edge detection

Edge detection is a classical method of image segmentation that still has some practical uses. In this study, it has been employed as a means of comparison with newer image segmentation techniques such as U-Net.

Fig. 3 illustrates the edge detection process followed in this study. Brightness and contrast adjustment techniques were utilized, along with noise reduction via a Gaussian filter. After noise reduction, the image is converted to grayscale, enabling the application of additional image processing techniques such as image binarization.

Once binarization is complete, edge detection will then be performed. The canny edge detector method was used in this study due to its superior detection capabilities. Detected edges were then represented on the original images to see how well the cracks and fractures were identified.

U-net semantic segmentation model

The U-Net deep learning model was selected for semantic segmentation in this study. The model architecture has a U-shaped structure as shown in Fig. 4. The U-Net has a contracting path (encoder), bottleneck layers at the bottom, and an expansive path (decoder).

Algorithm 2. : U-Net Sematic Segmentation Model

1. Input

- Image dataset $I = \{I_1, I_2, ..., I_n\}$, where each I_i is an input image.
- Mask dataset $M = \{M_1, M_2, ..., M_n\}$, where each M_i is a corresponding segmentation mask.
- Model parameters: Learning rate α, batch size B, number of epochs E.

2. Output

- Trained U-Net model f_θ capable of generating segmentation masks.

3. Procedure

1. Define U-Net architecture:
   - Contracting path (encoder)
     - Apply a series of convolutional layers with ReLU activation.
     - Use max pooling to downsample features at each level.
   - Bottleneck layer:
     - Apply convolutional layers with high-level feature extraction.
   - Expanding path (decoder)
     - Use transposed convolution to upsample feature maps.
     - Concatenate with corresponding encoder features (skip connections).
     - Apply convolutional layers to refine the segmentation map.
   - Final layer:
     - Use a 1×1 convolution to generate the segmentation mask output.
2. Train the U-Net model:
   - Initialize model weights and optimizer with learning rate α.
   - For each epoch e from 1 to E:
     - Iterate over batches of size B:
       - Load batch (I_b, M_b).
       - Perform forward pass: Compute predicted mask $\widehat{M}_b = f_\theta(I_b)$.
       - Compute loss function L (M_b, $\widehat{M}_b$).
       - Perform backpropagation and update model weights.
     - Evaluate model performance using validation data.
3. Save the trained model for inference.
4. Use the model for segmentation:
   - Given a new input image I_{new}, compute $\widehat{M}_{new} = f_\theta(I_{new})$.
   - Output the predicted mask $\widehat{M}_{new}$.

4. End Algorithm

convolutional block includes a (3,3) convolutional layer, ReLU activation, same padding, progressive dropout, and maxpooling filter of size (2,2).

The encoder choices aid in capturing intricate low-level features and high-level semantics. In convolutional layers, the dropout regularizes the model by preventing overfitting and promoting the learning of robust features. This helps prevent excessive co-adaptation of neurons and maintains the model's performance on unseen data. The iterative use of convolutional layers and max-pooling aids in the hierarchical abstraction of features, leading to a bottleneck layer that contains abstract representations. The expanding pathway restores spatial information using transposed convolution and ReLU-activated convolutional layers of size (2,2). Skip connections are integrated to establish connections between equivalent levels of the contracting and expanding pathways. U-Net's strategic connectedness enables the preservation of detailed spatial information and improves precise localization, which has been a key driver of its success in previous research. The choice of (3,3) convolutional layers in the decoder, along with dropout and extra convolutional layers, demonstrates a purposeful endeavor to enhance and expand feature representations. The final step involves a 1×1

Algorithm 2. above presents the pseudocode for the algorithm employed to configure the U-Net architecture. The encoder in a U-Net architecture captures important features of the input image at different levels of abstraction, starting from low-level details and progressing to high-level semantics. The contraction process involves input layers, convolutional layers, down sampling, dropouts, and ReLU activation functions to acquire contextual information. The input layer is set to 640×640 pixels with 3 color channels to enhance computational efficiency and preserve spatial image details. As the input advances through the encoder convolutional blocks, it undergoes spatial dimension reduction while extracting complex high-level information. Each

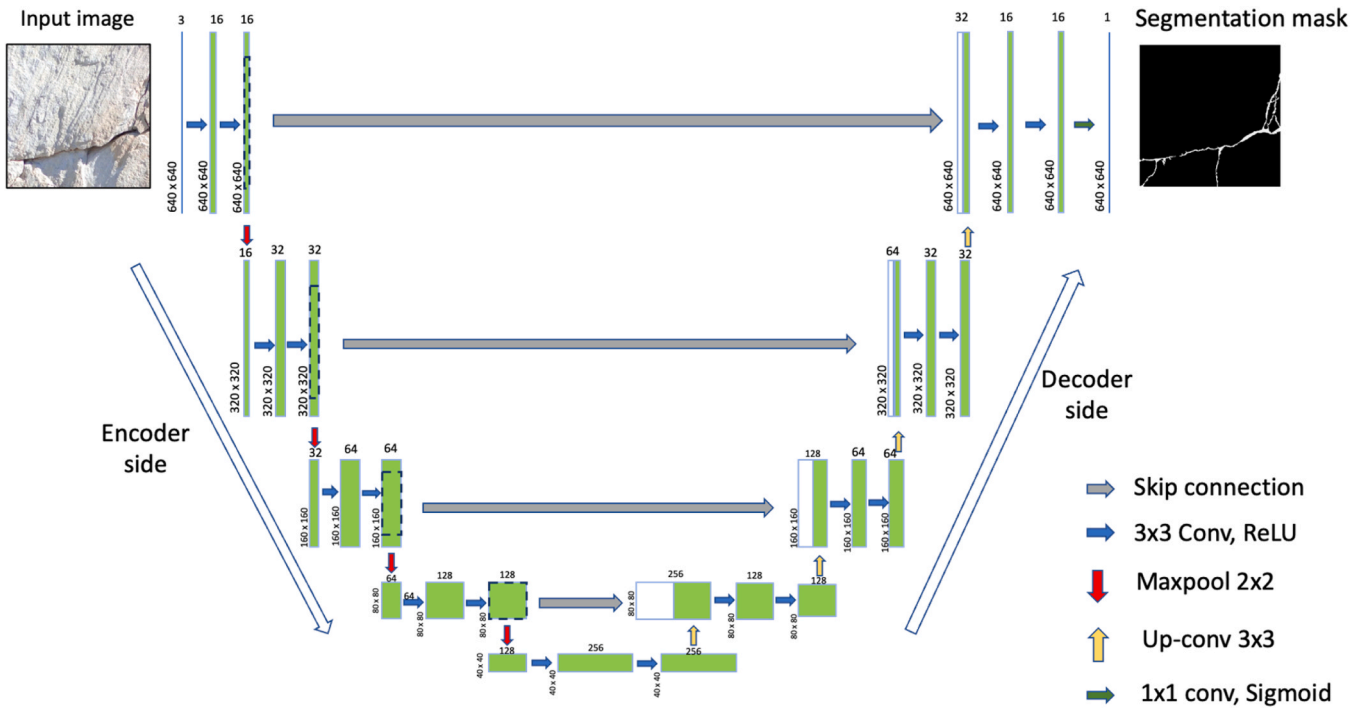

Fig. 4. U-Net model architecture.

convolutional layer with a sigmoid activation function, producing a binary segmentation mask for each pixel.

Hyperparameter selection and tuning significantly impact model performance. For the U-Net model architecture, hyperparameters like filter count, learning rate, number of epochs, and batch size. The contraction and expansion pathways, involving convolutional and transposed convolutional layers, necessitate meticulous adjustments to strike a balance between information retention and computational efficiency. Regularization techniques, like dropout, mitigate overfitting and improve the model's ability to generalize to unfamiliar data. The choice of loss function, cross-entropy, and optimizer, Adam, significantly impacts model training effectiveness. Evaluating a test dataset provides insights into the model's practical performance, leading to iterative adjustments of hyperparameters for a balanced trade-off between computational efficiency and prediction accuracy.

Model training

Training deep learning models is a demanding and time-consuming operation that necessitates a substantial amount of data. Gathering the data and fulfilling the pre-processing prerequisites, such as image cleansing and image annotation, further increases the time demands.

The first step is training the model on the original images that have

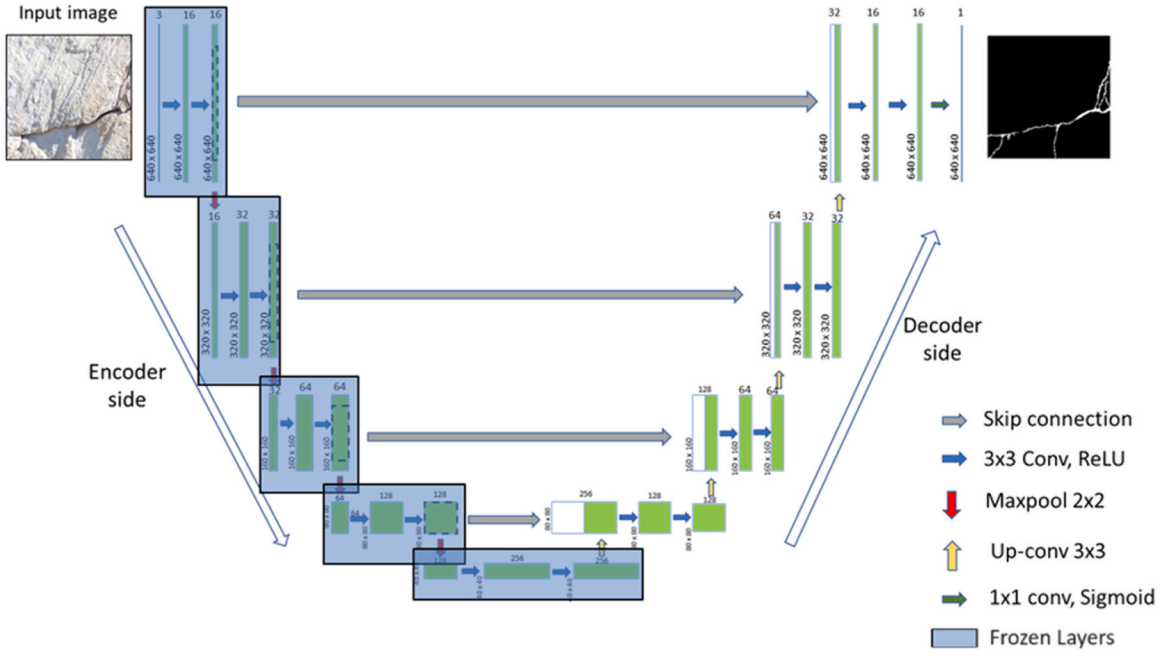

Fig. 5. A pretrained U-Net model with the frozen encoder layers and weights to prevent any further learning.

Table 2
The list of drones and camera sensors used for image data collection.

Drones	Features and Payload
Phantom 4 Pro	1-inch CMOS sensor 4 K/60fps videos, 20MP photos
Mavic Pro	1/2.3 in. CMOS sensor, 12.35MP photos
Matrice 100	The Zenmuse X5 camera was used in this study.

Table 3
A summary of drone flight missions for diverse data collection.

Flight	Drone	Batteries used	Images	Flight time (min)	Type	Time of day
1	Mavic Pro	2	806	28	Manual	10 am
2	Matrice 100	3	986	62	Auto, Manual	2:30 pm
3	Phantom 4	1	154	9	Auto	3:30 pm

already been through the pre-processing stages and are available for training. The hyperparameters described above will need to be adjusted over time to find the set of hyperparameters that together produce the best-trained model, that also performs well during the testing process. For the second training, the original images underwent image augmentation to increase the size of the dataset.

In the third technique, a pre-trained U-Net model will be used. A pre-trained model is a model that has been extensively trained on a large dataset to achieve a specific task. This model is later used in different, but related tasks. This approach is beneficial when the target task lacks annotated data. This is because the pre-trained model has already learned important features from the large dataset used during its initial training. Thus, it allows us to assess the accuracy and efficiency of our model even when trained on a smaller dataset.

The pre-trained U-Net model was trained on a dataset of 5000 images comprised of asphalt and concrete crack images. Post-training, the model's weights, and architecture were saved for subsequent transfer learning. Fig. 5 shows the process of using a pre-trained model. The encoder side of the model was frozen, preventing those model weights from undergoing any further training. New layers and weights were used for the decoder side of the model and then trained on the open pit highwall images.

Model evaluation

Model performance evaluation is crucial for assessing the effectiveness of deep learning architectures. This section explains the methods used for model evaluation, aiming to provide a thorough understanding of the metrics and techniques necessary for assessing the model's effectiveness. The evaluation metrics used include Intersection over Union (IoU). Eq. 2 shows how IoU is calculated, it measures the overlap between predicted and the ground truth segmentation masks.

$$IoU = \frac{TP}{TP + FP + FN} \tag{2}$$

The confusion matrix is crucial for a comprehensive analysis of model predictions, categorizing results into true positives (TP), true negatives (TN), false positives (FP), and false negatives (FN). The matrix plays a vital role in computing various metrics, including IoU, Precision (P_r), Recall (R_e), and F1 score shown in Eqs. (3), (4), and (5) respectively.

$$Precision(P_r) = \frac{TP}{TP + FP} \tag{3}$$

$$Recall(R_e) = \frac{TP}{TP + FN} \tag{4}$$

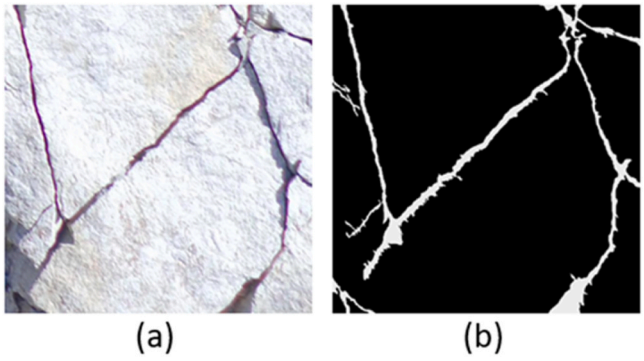

Fig. 6. (a) Original Image; (b) Segmentation Mask.

$$F1Score = \frac{2 \times Precision \times Recall}{Precision + Recall} \tag{5}$$

Results

This section discusses the results of a thorough study on crack and fracture detection on mine highwalls. To ensure that the chosen U-Net architecture was appropriate and its performance fairly evaluated, we considered alternative deep learning models during our initial study design. Based on literature and task-specific requirements, U-Net was selected due to its effectiveness in semantic segmentation and its ability to preserve spatial detail via skip connections. To promote comparison fairness and avoid bias toward a local optimum, we implemented three training strategies—original images, augmented images, and transfer learning with a pre-trained model—and compared all of them with a traditional Canny edge detector using standard evaluation metrics. This multi-strategy approach provides a robust basis for evaluating the model's segmentation performance.

Data collection and pre-processing

Table 2 provides the drones that were used to collect the image data for this study. Different camera sensors were used in this study to see if there would be a noticeable difference in crack and fracture detection from images collected using different drones. The image quality from all the drones was excellent and any differences were imperceptible upon inspection.

Table 3 outlines the various drone flight missions conducted during the data collection stage. The objective was to capture images at different times of the day, thereby diversifying the image dataset which is an important attribute of a robust training dataset.

After the collection of images, they undergo pre-processing steps based on the procedure described in section 4.2. Fig. 6(a) is one of the original images used as an input, while Fig. 6(b) shows the result of preprocessing applied to Fig. 6(a). The combination of the original image and the segmentation mask constitutes the dataset utilized in the training and testing processes.

Edge detection

Fig. 7 illustrates the edge detection process in various steps. In Fig. 7 (a), the original input images are presented. Fig. 7(b) depicts the initial stage of image enhancement, including adjustments to brightness and contrast, along with the application of a Gaussian filter for noise reduction. These initial steps diminish the prominence of background features, making them less detectable by edge detection techniques and thereby enhancing the visibility of foreground features. Subsequent steps involve histogram equalization and binarization. However, it was observed that histogram equalization was overly sensitive to

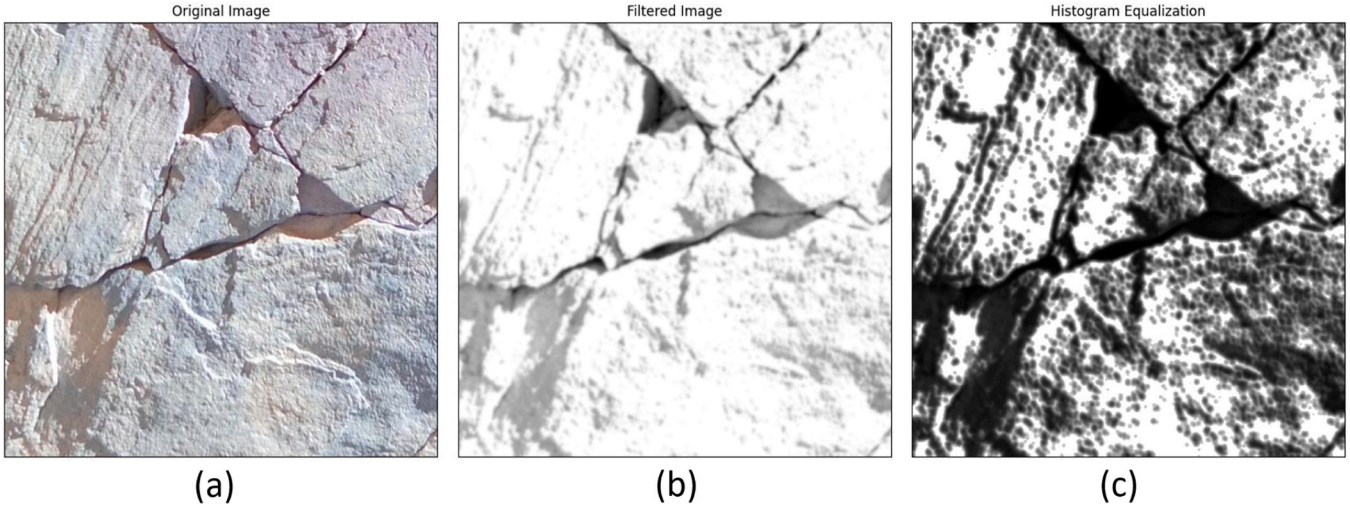

Fig. 7. (a) Original image; (b) Gaussian filter, brightness, and contrast; (c) Histogram equalization.

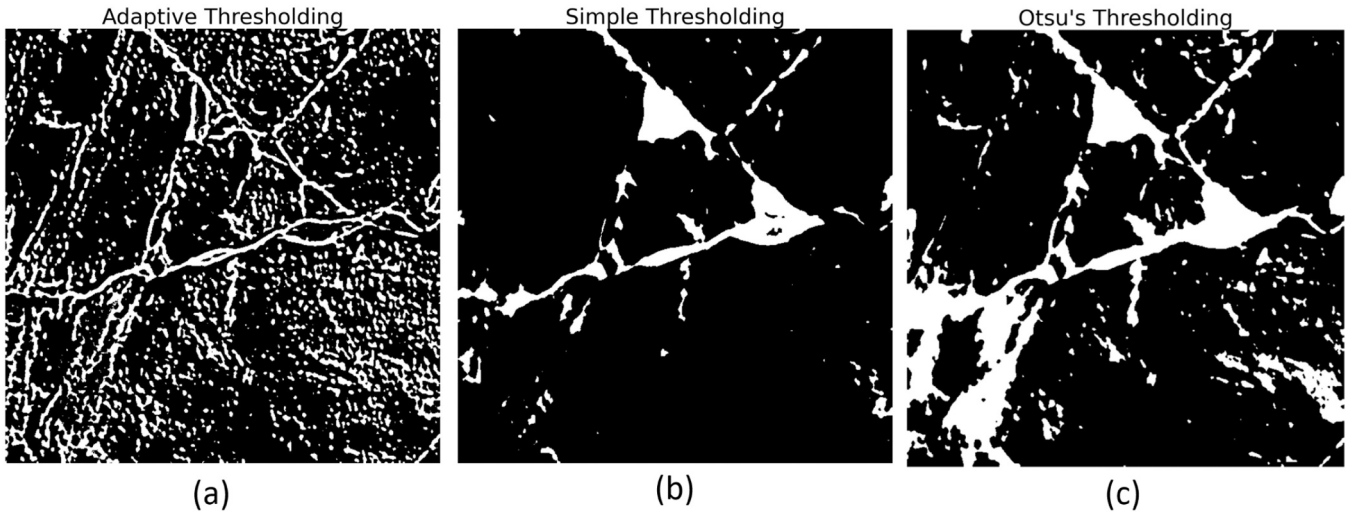

Fig. 8. Performance of different binarization methods.

background elements, leading to unwanted detections as indicated in Fig. 7(c).

Consequently, binarization proved to be a better option for most images compared to histogram equalization. Fig. 8 displays the outcomes of employing various thresholding methods. Adaptive thresholding, illustrated in Fig. 8(a), was preferable for certain images, while simple thresholding, shown in Fig. 8(b), was the most reliable method overall. The evaluation also included Otsu's binarization method, depicted in Fig. 8(c), to compare its effectiveness against the other techniques.

Edge detection was subsequently employed to isolate fractures and cracks. The Canny edge detector was used on binarized images, as shown in Fig. 9(a). After edge detection, as depicted in Fig. 9(b), the detected edges can be overlaid onto the original image. This overlay, illustrated in Fig. 9(c), allows for the assessment of how well the detected edges align with the observed cracks or fractures. The edge detection method demonstrated promising results, as seen in the visual output in Fig. 9 and its corresponding metrics. The drawback of using the edge detection methods is the need to adjust parameters for each processed image to achieve satisfactory segmentation results. This defeats the purpose of establishing an efficient framework for enhancing the current visual inspection methods.

U-net model training

Three different trainings were performed. To train the models, appropriate hyperparameters must be chosen. Table 4 summarizes the chosen hyperparameters for different training iterations under each training. The image data was randomly split into two categories: 80 % and 20 % for the training and testing sets, respectively. A modest 100 annotated images were used in the first training.

The optimal training run for the first training was conducted for 20 epochs, adhering to the early stopping protocol. This protocol monitors the validation loss and terminates the training if there is no improvement for 4 consecutive epochs. High accuracy was observed in both testing and training, reaching approximately 97 %. Fig. 10 shows a noticeable performance gap exists between the training and validation sets, with losses converging at 0.22 and 0.14, respectively. This gap is caused by the limited number of input images.

The second training used the same U-Net architecture model. Data augmentation was applied to 100 images, expanding the dataset to 1000 images. Additionally, a few hyperparameters were modified. The batch size was set to 15, the learning rate was adjusted to 0.0015, and the model was trained for 40 epochs, again coming to an early stop due to the early stopping protocol. Fig. 11 shows the loss and accuracy achieved during training. The training and validation accuracy is in the high

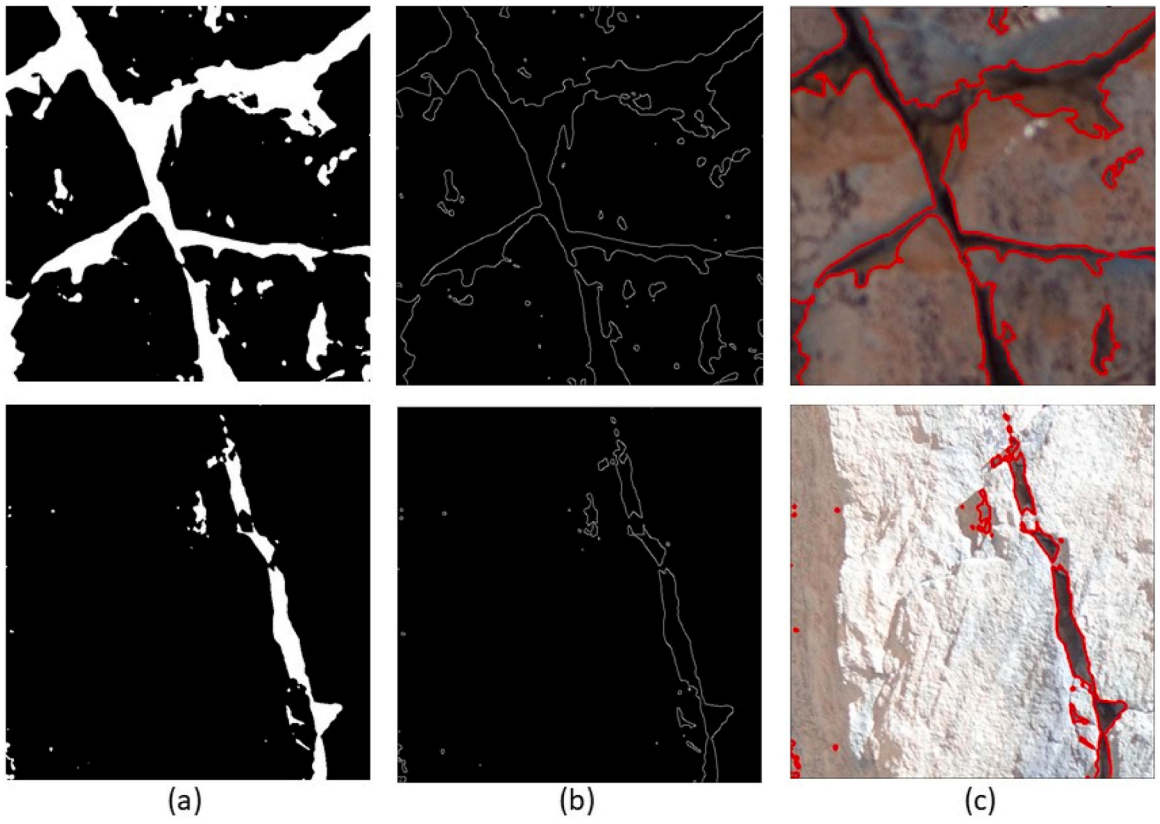

Fig. 9. (a) Binary image; (b) Edges detected; (c) Prominent edges overlaid on the original image.

Table 4
Hyperparameter selection for different trainings.

Hyperparameter	First Training Train on original images	Second Training Train on the augmented images	Third training Pre-Trained model
Input Size	(640, 604, 3)	(640, 604, 3)	(640, 604, 3)
Dropout	0.1–0.3	0.1–0.3	0.1–0.3
Loss Function	Binary Crossentropy	Binary Crossentropy	Binary Crossentropy
Optimizer	Adam	Adam	Adam
Learning Rate	0.001	0.0015	0.001
Batch Size	5	15	15
No. Epochs	30	40	15
Early Stopping	Val_loss, patience= 4 epochs	Val_loss, patience= 2 epochs	Val_loss, patience= 4 epochs

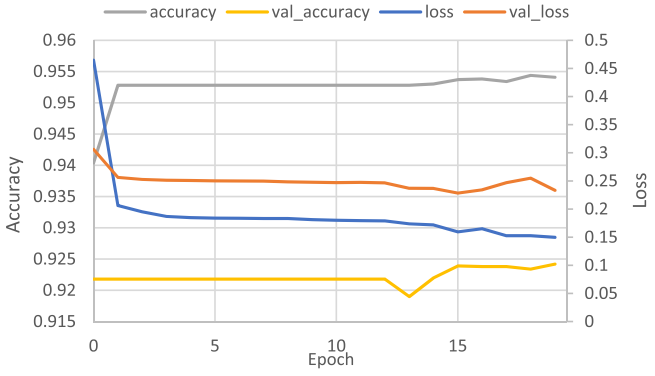

Fig. 10. Training and validation loss and accuracy for first training.

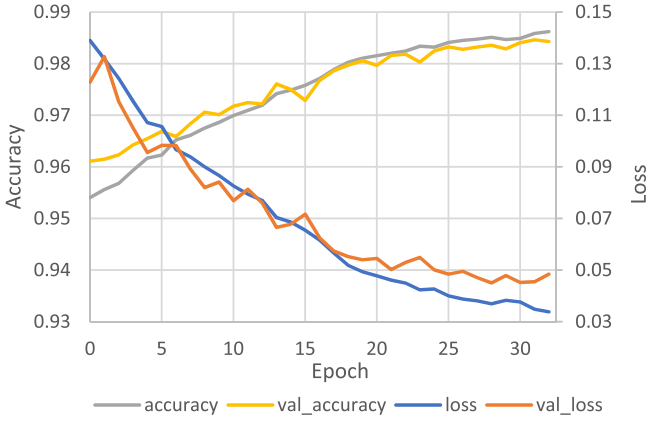

Fig. 11. Training and validation loss and accuracy for second training.

98 %, which is expected in image segmentation tasks with prominently represented backgrounds. The training and validation loss shows convergence, indicating that the model generalizes well to unseen data. Additional model evaluation techniques will be explored to assess the relative performance of the models.

Another option considered was employing a pre-trained U-Net model. For the third training, the U-Net model architecture mentioned earlier was initially trained on the dataset described in section ↱4.4.1. Fig. 12 presents the training and validation loss and accuracy curves for the third training using the pre-trained U-Net model. Transfer learning was implemented to train the pre-trained model on our dataset of 1000 images comprised of original and augmented images. The training setup included 15 epochs, a batch size of 15, and a learning rate of 0.001. Both training and validation accuracy increased to approximately 97 %. The loss showed convergence, decreasing for both training and validation.

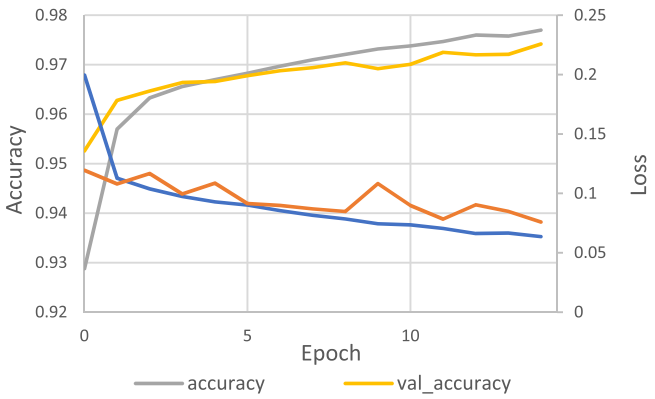

Fig. 12. Training and validation loss and accuracy for third training.

Table 5
Performance metrics.

Methods	Pr	Re	F1	IoU
First training	0.7014	0.1399	0.2206	0.5397
Second training	0.7733	0.6645	0.6993	0.7706
Third training	0.7213	0.4878	0.5597	0.6928
Edge Detection	0.6968	0.7329	0.7072	0.7504

This suggests that the model may generalize well to unseen data. This was confirmed when the model achieved 97 % accuracy on 220 new images, consistent with training and validation.

Model evaluation

To assess model performance, four metrics, including precision, recall, F1 score, and IoU, were employed, as defined in section ↱4.5. These metrics were computed using a confusion matrix, which categorizes predictions into true positives (TP), true negatives (TN), false positives (FP), and false negatives (FN) by comparing the predicted segmentation mask with the ground truth from human annotation.

Table 5 outlines the performance of the different models' iterations trained. Having an adequate large dataset is an important part of training deep learning models. The U-Net model trained in second training showed the best performance among the deep learning models with the highest F1 score and IoU. Besides numerical metrics, it is crucial to analyze the visual outcomes in the form of segmentation masks produced by these models.

In this study, high-resolution images were captured from the quarry and divided into smaller patches for segmentation. This approach was chosen to ensure computational efficiency and to effectively manage the large image sizes while preserving the essential crack and fracture features. By evaluating segmentation performance on these patches, the study demonstrated the model's ability to generalize well across different regions of the highwall.

The visual output of the different trainings can be seen in Fig. 13. Visual inspection of the output segmentation masks provides valuable insights into the U-Net model's performance and areas of improvement. These insights can be utilized to enhance the model in subsequent training iterations by improving the dataset. The visual output obtained from the different trainings is in concert with the performance metrics in that the U-Net models trained in second and third trainings show great segmentation masks that localize the fractures and cracks well. Fig. 13 provides a comprehensive visual comparison essential for evaluating the performance of the U-Net model across different trainings. It presents the original image (a) as the baseline for comparison, alongside the ground truth (b), representing the ideal segmentation outcome. The subsequent parts of the figure show the output segmentation masks generated by the model under three distinct trainings: First training (c), Third training (d), and Second training (e).

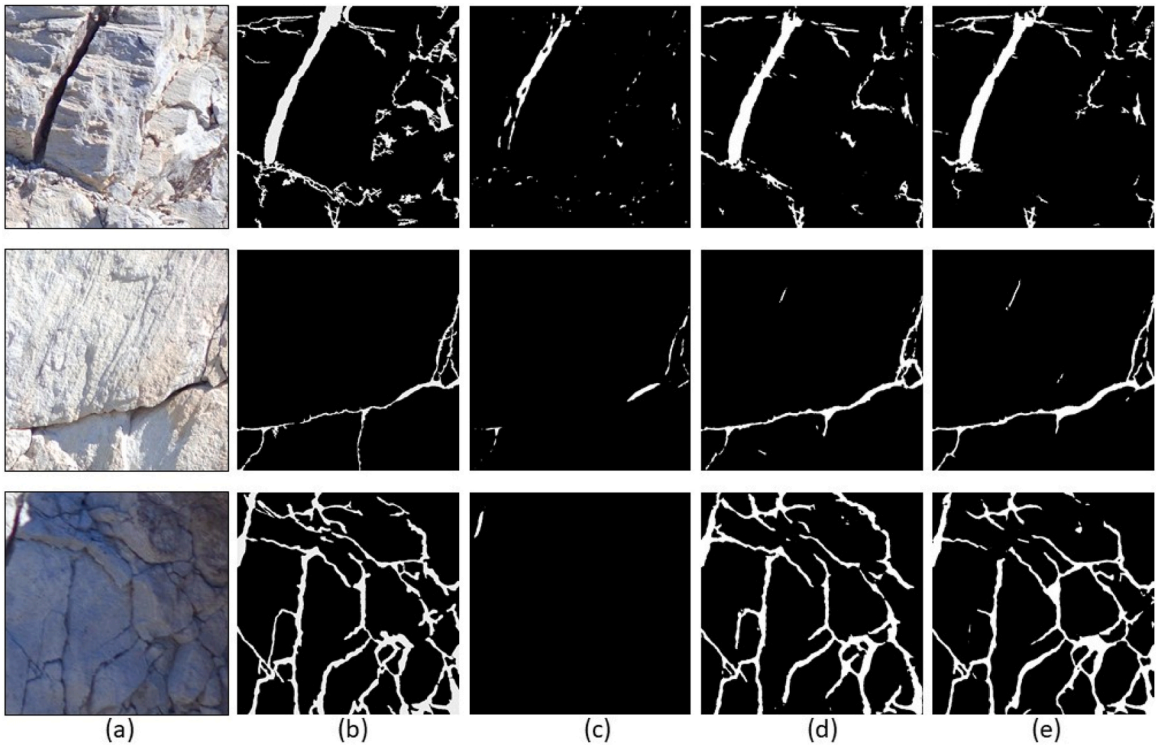

Fig. 13. Comparison of predicted segmentation masks from the various trainings. (a) Original image; (b) ground truth (c) First training; (d) Third training; (e) Second training.

Conclusion

A U-Net model was developed to dynamically detect cracks on open pit mine highwalls, augmenting the existing method of human visual inspections. Three distinct trainings were established to assess the model, each with its own dynamic impact based on the availability of data. The first training involved training the model on a modest dataset consisting of 100 images. In the second training, the model was trained with a dataset of 1000 images that included both original and augmented images. The third training utilized transfer learning and fine-tuning, where a deep learning model was built on a distinct yet interconnected dataset. Specifically, the model was trained on images depicting cracks and fractures in concrete and asphalt. The pre-trained model was adapted to train on the highwall image dataset, leveraging the insights acquired from previous training to enhance the learning of the characteristics of the present dataset. Furthermore, a conventional edge detection technique was employed to contrast the newer deep learning approaches with the more traditional pixel-wise detection methods. The optimal training setup of second training, yielded a precision of 77.33 %, recall of 66.45 %, and IoU of 77.06 %. The IoU metric is highly effective in evaluating the model's ability to accurately locate fractures and cracks in the image. The model successfully segments cracks and fractures. The crack semantic segmentation method exhibits significant promise for practical implementation. Once the model is trained and deployed, it offers an intuitive approach to locating cracks and fractures.

Future work may expand this study by incorporating images from multiple mining operations with varied rock types and textures to enhance the training dataset. Evaluating the model's performance on full-resolution panoramic images will provide a more comprehensive assessment of its robustness. Additionally, exploring emerging deep learning architectures could further improve segmentation accuracy.

CRediT authorship contribution statement

Letshwiti Tebogo M.: Writing – original draft, Methodology, Investigation, Formal analysis, Conceptualization. **Sattarvand Javad:** Validation, Supervision, Funding acquisition, Conceptualization. **Shahsavar Mahdi:** Writing – review & editing, Data curation, Conceptualization. **Moniri-Morad Amin:** Writing – review & editing, Validation.

Declaration of Competing Interest

The authors declare that they have no known competing financial interests or personal relationships that could have appeared to influence the work reported in this paper.

Acknowledgments

Research conducted at the Automation Laboratory of University of Nevada, Reno (UNR) under a grant Called "Artificially Intelligent Mining Systems for safer and healthier automated operations" sponsored by the National Institute of Occupational Safety and Health (NIOSH) under contract number #75030119C06044.

References

[1] H.L. Hartman, J.M. Mutmansky, Introductory Mining Engineering, J. Wiley, Hoboken, N.J, 2002.
[2] S. Kumar, A.K. Mishra, B.S. Choudhary, Prediction of back break in blasting using random decision trees, Eng. Comput. 38 (Jun. 2022) 1185–1191, https://doi.org/10.1007/s00366-020-01280-9.
[3] L.J. Carlos, L.J. Emilio, J.A.C. Francisco, R. Yvonne Visser de. Drilling and Blasting of Rocks, 1st ed, CRC Press, London, 1987, https://doi.org/10.1201/9781315141435.
[4] K.S. Osasan, T.B. Afeni, Review of surface mine slope monitoring techniques, J. Min. Sci. 46 (2) (2010) 177–186, https://doi.org/10.1007/s10913-010-0023-8.
[5] S. Nunoo, D.D. Tannant, H.W. Newcomen, Slope monitoring practices at open pit porphyry mines in British Columbia, Canada, Int J. Min. Reclam. Environ. 30 (3) (May 2016) 245–256, https://doi.org/10.1080/17480930.2015.1038865.
[6] J.M. Girard and E. Mchugh, "Detecting problems with mine slope stability," 2000, Accessed: Mar. 24, 2024. [Online]. Available: ⟨https://stacks.cdc.gov/view/cdc/8679⟩.
[7] Extensometers," ⟨https://sisgeo.com/products/extensometers/⟩.
[8] N.Q. Long, et al., Accuracy assessment of mine walls' surface models derived from terrestrial laser scanning, Int J. Coal Sci. Technol. 5 (3) (2018) 328–338, https://doi.org/10.1007/s40789-018-0218-1.
[9] A. Kamran-Pishhesari, A. Moniri-Morad, J. Sattarvand, Applications of 3D reconstruction in virtual reality-based teleoperation: a review in the mining industry, Technol. (Basel) 12 (3) (2024) 40.
[10] E. Marsh, J. Dahl, A. Kamran Pishhesari, J. Sattarvand, F.C. Harris Jr, A Virtual Reality Mining Training Simulator for Proximity Detection, in International Conference on Information Technology-New Generations, Springer, 2023, pp. 387–393.
[11] C. Xiao, R. Yang, X. Ma, Y. Wang, C. Ding, Damage evaluation of rock blasting based on multi-fractal study, Int J. Impact Eng. (2024) 104953.
[12] T. Bamford, F. Medinac, K. Esmaeili, Continuous monitoring and improvement of the blasting process in open pit mines using unmanned aerial vehicle techniques, Remote Sens (Basel) 12 (Aug. 2020) 34, https://doi.org/10.3390/rs12172801.
[13] J.A. Gomez Llerena, M. Ghahramanieisalou, J. Sattarvand, Tackling Geotechnical Risks in Tailings Dams Using High-Resolution UAV Imaging and Advanced Image Processing, American Society of Civil Engineers (ASCE), Jul. 2023, pp. 220–228, https://doi.org/10.1061/9780784484975.024.
[14] R. Battulwar, et al., A practical methodology for generating high-resolution 3D models of open-pit slopes using UAVs: flight path planning and optimization, Remote Sens (Basel) 12 (14) (Jul. 2020), https://doi.org/10.3390/rs12142283.
[15] F. Alzubaidi, P. Mostaghimi, G. Si, P. Swietojanski, R.T. Armstrong, Automated rock quality designation using convolutional neural networks, Rock. Mech. Rock. Eng. 55 (6) (Jun. 2022) 3719–3734, https://doi.org/10.1007/s00603-022-02805-y.
[16] Y. Xu, Y. Fan, Y. Bao, H. Li, Task-aware meta-learning paradigm for universal structural damage segmentation using limited images, Eng. Struct. 284 (2023) 115917.
[17] Y. Xu, Y. Fan, H. Li, Lightweight semantic segmentation of complex structural damage recognition for actual bridges, Struct. Health Monit. 22 (5) (2023) 3250–3269.
[18] Y. Xu, et al., A modified U-net for crack segmentation by Self-Attention-Self-Adaption neuron and random elastic deformation, Smart Struc. Syst. Int. J. 29 (1) (2022) 1–16.
[19] J. Valencia, J. Sattarvand, E. Emami, Support vector machine and convolutional neural networks applied to blasthole detection over photogrammetry representations, Appl. Comput. Oper. Res. Miner. Ind., APCOM 202 (2022).
[20] B. Peik, et al., An Analytical Study of Rockfall Trajectory Simulation to Develop Hazard Maps for Open-Pit Mines, American Rock Mechanics Association, 2020.
[21] O. Ronneberger, P. Fischer, T. Brox, U-Net: Convolutional Networks for Biomedical Image Segmentation, May 2015, [Online]. Available: ⟨http://arxiv.org/abs/1505.04597⟩.
[22] S. Bhattiprolu, python_for_microscopists, ⟨https://github.com/bnsreenu/python_for_microscopists/blob/master/204-207simple_unet_model.py⟩.
[23] R. Singh, R. Rani, Semantic segmentation using deep convolutional neural network: a review, SSRN Electron. J. (2020), https://doi.org/10.2139/ssrn.3565919.
[24] S. Minaee, Y. Boykov, F. Porikli, A. Plaza, N. Kehtarnavaz, D. Terzopoulos, Image segmentation using deep learning: a survey, IEEE Trans. Pattern Anal. Mach. Intell. 44 (7) (Jul. 2022) 3523–3542, https://doi.org/10.1109/TPAMI.2021.3059968.
[25] F. Alzubaidi, P. Makuluni, S.R. Clark, J.E. Lie, P. Mostaghimi, R.T. Armstrong, Automatic fracture detection and characterization from unwrapped drill-core images using mask R–CNN, J. Pet. Sci. Eng. 208 (Jan. 2022), https://doi.org/10.1016/j.petrol.2021.109471.
[26] G. Winkelmaier, R. Battulwar, M. Khoshdeli, J. Valencia, J. Sattarvand, B. Parvin, Topographically guided UAV for identifying tension cracks using image-based analytics in open-pit mines, IEEE Trans. Ind. Electron. 68 (6) (Jun. 2021) 5415–5424, https://doi.org/10.1109/TIE.2020.2992011.
[27] M. Monjezi, H. Amini Khoshalan, A. Yazdian Varjani, Prediction of flyrock and backbreak in open pit blasting operation: a neuro-genetic approach, Arab. J. Geosci. 5 (3) (Aug. 2010) 441–448, https://doi.org/10.1007/s12517-010-0185-3.
[28] R. Shirani Faradonbeh, M. Monjezi, D. Jahed Armaghani, Genetic programing and non-linear multiple regression techniques to predict backbreak in blasting operation, Eng. Comput. 32 (1) (Jan. 2016) 123–133, https://doi.org/10.1007/s00366-015-0404-3.
[29] A. Saghatforoush, M. Monjezi, R. Shirani Faradonbeh, D. Jahed Armaghani, Combination of neural network and ant colony optimization algorithms for prediction and optimization of flyrock and back-break induced by blasting, Eng. Comput. 32 (2) (Apr. 2016) 255–266, https://doi.org/10.1007/s00366-015-0415-0.
[30] E. Ebrahimi, M. Monjezi, M.R. Khalesi, D.J. Armaghani, Prediction and optimization of back-break and rock fragmentation using an artificial neural network and a bee colony algorithm, Bull. Eng. Geol. Environ. 75 (1) (Feb. 2016) 27–36, https://doi.org/10.1007/s10064-015-0720-2.
[31] M. Esmaeili, M. Osanloo, F. Rashidinejad, A. Aghajani Bazzazi, M. Taji, Multiple regression, ANN and ANFIS models for prediction of backbreak in the open pit blasting, Eng. Comput. 30 (4) (Oct. 2014) 549–558, https://doi.org/10.1007/s00366-012-0298-2.

[32] M. Monjezi, H. Dehghani, Evaluation of effect of blasting pattern parameters on back break using neural networks, Int. J. Rock. Mech. Min. Sci. 45 (8) (2008) 1446–1453, https://doi.org/10.1016/j.ijrmms.2008.02.007.
[33] E. Ghasemi, Particle swarm optimization approach for forecasting backbreak induced by bench blasting, Neural Comput. Appl. 28 (7) (Jul. 2017) 1855–1862, https://doi.org/10.1007/s00521-016-2182-2.
[34] J. Zhou, Y. Dai, M. Khandelwal, M. Monjezi, Z. Yu, Y. Qiu, Performance of hybrid SCA-RF and HHO-RF models for predicting backbreak in open-pit mine blasting operations, Nat. Resour. Res. 30 (6) (Dec. 2021) 4753–4771, https://doi.org/10.1007/s11053-021-09929-y.
[35] Z. Nabavi, M. Mirzehi, H. Dehghani, P. Ashtari, A hybrid model for back-break prediction using XGBoost machine learning and metaheuristic algorithms in chadormalu iron mine, J. Min. Environ. 14 (2) (Apr. 2023) 689–712, https://doi.org/10.22044/jme.2023.12796.2323.
[36] M. Mohammadnejad, R. Gholami, F. Sereshki, A. Jamshidi, A new methodology to predict backbreak in blasting operation, Int. J. Rock. Mech. Min. Sci. 60 (2013) 75–81, https://doi.org/10.1016/j.ijrmms.2012.12.019.
[37] A. Sayadi, M. Monjezi, N. Talebi, M. Khandelwal, A comparative study on the application of various artificial neural networks to simultaneous prediction of rock fragmentation and backbreak, J. Rock. Mech. Geotech. Eng. 5 (4) (2013) 318–324, https://doi.org/10.1016/j.jrmge.2013.05.007.
[38] J. Jing, S. Liu, G. Wang, W. Zhang, C. Sun, Recent advances on image edge detection: a comprehensive review, Neurocomputing 503 (2022) 259–271, https://doi.org/10.1016/j.neucom.2022.06.083.
[39] D. Ziou, … S. T.-R and I. A. A in, and undefined 1998, Edge detection techniques-an overview, inria.hal.scienceD Ziou, S TabboneРаспознавание образов и анализ изображЖен/Pattern Recognition and Image, 1998•inria.hal.science, Accessed: Mar. 24, 2024. [Online]. Available: ⟨https://inria.hal.science/inria-00098446/⟩.
[40] G. Shrivakshan, C. C.-I. J of Computer, and undefined 2012, A comparison of various edge detection techniques used in image processing, CiteseerGT Shrivakshan, C ChandrasekarInternational Journal of Computer Science Issues (IJCSI), 2012•Citeseer, 2012, Accessed: Mar. 24, 2024. [Online]. Available: ⟨https://citeseerx.ist.psu.edu/document?repid=rep1&type=pdf&doi= 685e8ecc44034 3d59f157ca1add377b956b2199d⟩.
[41] E.Igbinosa Ireyuwa, Comparison of edge detection technique in image processing techniques, Int. J. Inf. Technol. Electr. Eng. 2 (1) (2013) 25–29.
[42] P. Janani, J. Premaladha, K.S. Ravichandran, Image enhancement techniques: a study, Indian J. Sci. Technol. 8 (22) (2015), https://doi.org/10.17485/ijst/2015/v8i22/79318.
[43] A. Huamán, Basic Thresholding Operations, ⟨https://docs.opencv.org/4.x/db/d8e/tutorial_threshold.html⟩.